



Cite this: *RSC Adv.*, 2023, 13, 6065

# Preparation, characterization, and energy simulation of ZnTiO<sub>3</sub> high near-infrared reflection pigment and its anti-graffiti coating†

Song Wang,  Jihu Wang,\* Shaoguo Wen, Hui Li, Chen Xie, Shuaibiao Li and Dajiang Mei

In the field of cooling materials, ZnTiO<sub>3</sub> (ZT) is still a new member that needs to be further studied. In this paper, pure cubic ZT was synthesized by the sol–gel method, and the effect of calcination temperature on ZT synthesis was investigated. The hydrophobic modification was carried out on ZT to prepare near-infrared reflective thermal insulation functional composite coatings based on silicone resin (SI). Compared with unmodified ZT (U-ZT), the modified ZT (M-ZT) exhibits better dispersion in the SI matrix, contributing to improved solar reflectance and anti-graffiti performance. The EnergyPlus software was used to simulate energy consumption in the air conditioning system. The excellent chemical stability and high NIR reflectance made the synthesized pigments potential candidates for energy-saving coatings. The simulation showed that homeowners could save \$10.29 a month by applying an energy-efficient coating consisting of ZT to the walls and roofs of their buildings. Besides, these coatings show potential anti-graffiti application due to the exceptional repellency of coated surfaces against water-based ink, oily red marker, and paint.

Received 12th December 2022  
Accepted 11th February 2023

DOI: 10.1039/d2ra07903h

rsc.li/rsc-advances

## 1 Introduction

Nowadays, with the increasingly severe problem of global warming, how to reduce energy consumption, curb the energy crises, and achieve sustainable development of the earth has become a hot topic of current research. It is reported that about 40–50% of global energy of the construction industry was consumed with summer cooling and winter heating per year.<sup>1</sup> Energy consumption in large cities significantly exacerbates this effect.<sup>2</sup> It is well known that solar radiation consists of 5% ultraviolet radiation (UV: 300–400 nm), 43% visible light (vis: 400–800 nm), and 52% near-infrared radiation (near-infrared: 800–2500 nm).<sup>3</sup> The heat is generated mainly in the near-infrared region. Therefore, the passive cooling coating has become one of the effective methods to solve the problem of energy consumption.<sup>4–6</sup> It has high solar reflectivity and thermal emissivity, thus significantly reducing the conversion of solar energy into heat energy. To solve the low reflection characteristics of polymers, functional fillers including TiO<sub>2</sub> (ref. 7 and 8) and ZnO<sup>9</sup> are usually added to them for modification.

White coatings filled with TiO<sub>2</sub> and ZnO are widely used in architectural coatings due to their low cost and high thermal stability. But the reflectivity is easy to decline after dirtying and

pollution. In order to maintain the high near-infrared reflectivity of coatings, the hydrophobic surface can provide anti-fouling and self-cleaning properties.<sup>10</sup>

Recently, perovskite zinc titanate (ZT) has been investigated due to its wide range of applications in microwave dielectrics, sorbents for the desulfurization of hot coal gases, and gas sensors.<sup>11–13</sup> Compared with the band gap of ZnO and TiO<sub>2</sub>, ZT has a higher value, and the electron mobility of ZT is about 150 to 400 cm<sup>2</sup> V<sup>−1</sup> s<sup>−1</sup>.<sup>14</sup> ZT is a candidate for passive cooling coatings.

Silicone resin (SI) is a colorless and transparent polymer with many attractive properties such as chemical stability, high-temperature resistance, excellent mechanical strength, and biocompatibility<sup>15,16</sup> because of Si–O bonds. Due to these outstanding excellent properties, SI has been widely used in protective coatings, films, and flexible electronics.<sup>17–19</sup> SI is an ideal material for a variety of outdoor applications. However, the lower solar reflectance of SI severely limits its application in the field of reflective thermal insulation coatings. Inorganic particles with high solar reflectance are usually used in polymer–inorganic hybrid composites, which can significantly solve the problem of low reflectance for infrared light.<sup>20</sup> Therefore, SI was used as the resin in this paper to improve the hydrophobicity and mechanical strength of the superhydrophobic coating.

Unfortunately, most ceramics are hydrophilic due to the presence of hydroxyl (–OH) groups on their surfaces.<sup>21</sup> For polymer–inorganic hybrid composites, the high quality ratio

College of Chemistry and Chemical Engineering, Shanghai University of Engineering Science, Shanghai 201620, PR China. E-mail: wangjihu@163.com

† Electronic supplementary information (ESI) available. See DOI: <https://doi.org/10.1039/d2ra07903h>



between inorganic powder and organic polymer leads to agglomeration in the polymer matrix.<sup>22</sup> Surface hydrophobic modification of inorganic nanoparticles can effectively improve its dispersion stability in polymer matrices and the self-cleaning performance of the coating.<sup>23–25</sup>

In this paper, our research attempts to develop a strategy for lowering the sintering temperature and time for the crystallization of nanostructured zinc titanate material by employing a suitable aqueous particulate sol-gel route rather than the polymeric sol-gel methods reported previously. Using an aqueous solution instead of a polymer solution makes the preparation process environmentally friendly. This method is a simple and cheap process with a fast preparation rate. The effect of sintering temperature on the physical and chemical properties of prepared powders was investigated.

Stearic acid was applied to conduct the hydrophobic modification on the surface of ZT by the physical coating method. On this basis, SI/ZT composite membrane was prepared. The coating has excellent chemical resistance and anti-graffiti properties. In addition, to the best of our knowledge, there is limited literature on exploring solar reflective coatings with ZT as the cooling coating. Jinpeng Lv *et al.*<sup>26</sup> hexagonal ZT was synthesized by high temperature solid state method. However, too high calcination temperature (800 °C) leads to a large particle size of ZT (between 100 nm and 1 μm), which will have a serious impact on the dispersion of powder in the coating and reduce the reflection performance of the coating. Only the performance of ZT powder has been studied, but the performance of the coating has not been studied. In addition, ZT powder has poor reflectivity in the near-infrared region. Thus, this work aims to the scale-up synthesis of hexagonal ZT pigments and special attention will be paid to the exploration of roof cooling and self-cleaning effects.

## 2 Experimental section

### 2.1 Materials

Zinc nitrate hexahydrate ( $\text{Zn}(\text{NO}_3)_2 \cdot 6\text{H}_2\text{O}$ , 99%), titanium(IV) butoxide ( $\text{Ti}(\text{OC}_4\text{H}_9)_4$ , 99%), citric acid (99.5%), stearic acid (99%), tetrahydrofuran (THF, 99.5%), anhydrous ethanol ( $\text{EtOH}$ , 99.7%) were all of analytical and purchased from Shanghai Titan Technology Co., Ltd. Silicone resin (Hangzhou Qianyang Technology Co., Ltd). Deionized water was homemade.

### 2.2 Synthesis of ZT nanoparticles

The ZT nanoparticles were synthesized by sol-gel method using  $\text{Zn}(\text{NO}_3)_2 \cdot 6\text{H}_2\text{O}$ ,  $\text{Ti}(\text{OC}_4\text{H}_9)_4$  as starting materials, and citric acid anhydrous as chelating agent. At first, 0.08 mol from citric acid anhydrous and 0.02 mol from  $\text{Ti}(\text{OC}_4\text{H}_9)_4$  were dissolved in deionized water, then mixed in a bunsen beaker. The obtained solution was heated and stirred at 60 °C in a constant temperature magnetic stirrer with total reflux of 1 h until  $\text{Ti}(\text{OC}_4\text{H}_9)_4$  was completely dissolved. Then,  $\text{Zn}(\text{NO}_3)_2 \cdot 6\text{H}_2\text{O}$  was mixed with the above solution. The ratio of citric acid anhydrous to metallic cations was constant and equal to 2 : 1. The ammonia

was dropped into the mixed solution to modulate the pH value to 1–2. The transparent sol was gradually formed and then heated to 120 °C for 12 h. A brown puffy porous gel was obtained. The dry precursors were ground into powders, then pretreated by heating at 500 °C for 6 h. Finally, the resulting powders were calcined at three temperatures 600 °C, 700 °C, 800 °C, 850 °C, and 900 °C for 3 h (Fig. 1a).

### 2.3 Surface modification of ZT

Because the surface of ZT is hydrophilic, stearic acid was used to modify ZT by the physical coating method. First, 0.1 g stearic acid was dispersed into 20 mL of ethanol under magnetic stirring at 60 °C for 10 min until stearic acid was completely dissolved. Second, 2 g ZT was appended to the beaker to continue the process for 30 min. Finally, the ethanol solution was dried at 60 °C under air for 2 h. Stearic acid is almost completely coated on the ZT. The surface modification ZT (M-ZT) was obtained (Fig. 1b).

### 2.4 Preparation of SI/M-ZT composite film

The M-ZT was mixed in 4 mL tetrahydrofuran and dispersed by ultrasonic for 20 min. The mixed solution of M-ZT and tetrahydrofuran was then poured into SI, the addition amount of M-ZT is 5 wt%, 10 wt%, 15 wt%, 20 wt% and 30 wt% of SI respectively. Stirring for another 1 h at 700 rpm. The aluminum plate was used as the substrate. Before use, it was polished with 400 mesh sandpaper and ultrasonically cleaned with ethanol and acetone to remove pollutants. Under the condition of 30% relative humidity and 25 °C, the corresponding films were prepared by a roller coating method. After curing for 24 h at ambient temperature, the hydrophobic reflective insulation M-ZT composite films with a thickness of 100 μm were obtained.

### 2.5 Characterization

The XRD patterns of the ZT powders calcined at different temperatures were collected by an X-ray diffractometer (Bruker D8 Advance 40 kV, 40 mA). Scanning electron microscopy (SEM, Sigma 300, Zeiss, Japan) was used to analyze the fractured surfaces of SI and ZT/SI composite film. Static contact angle and surface tension of unmodified ZT (U-ZT), M-ZT, SI, and ZT/SI composite film were measured by a water contact angle tester (Shanghai Pushen Testing instrument). UV-VIS-NIR spectrophotometer (UV3600 with an integrating sphere attachment, Shimadzu, Japan) was used to test the reflectance spectra of the ZT and ZT films. X-ray photoelectron spectroscopy (Thermo ESCALAB 250XI, America). High-low temperature alternating test chambers (GDJS-100C, Guangzhou Biuged Laboratory Instrument Things Co., Ltd) and ultraviolet aging test chamber (BGD 866/A, Guangzhou Biuged Laboratory Instrument Things Co., Ltd) were applied to study the antiaging of SI and ZT/SI composite film.

Anti-graffiti analysis of ZT/SI film. The specific test steps are as follows: ink, oil-based marker, and black spray paint separately were used to paint (spray) a 20 mm × 20 mm mark on the center of the coated surface of the test panel, three panels in



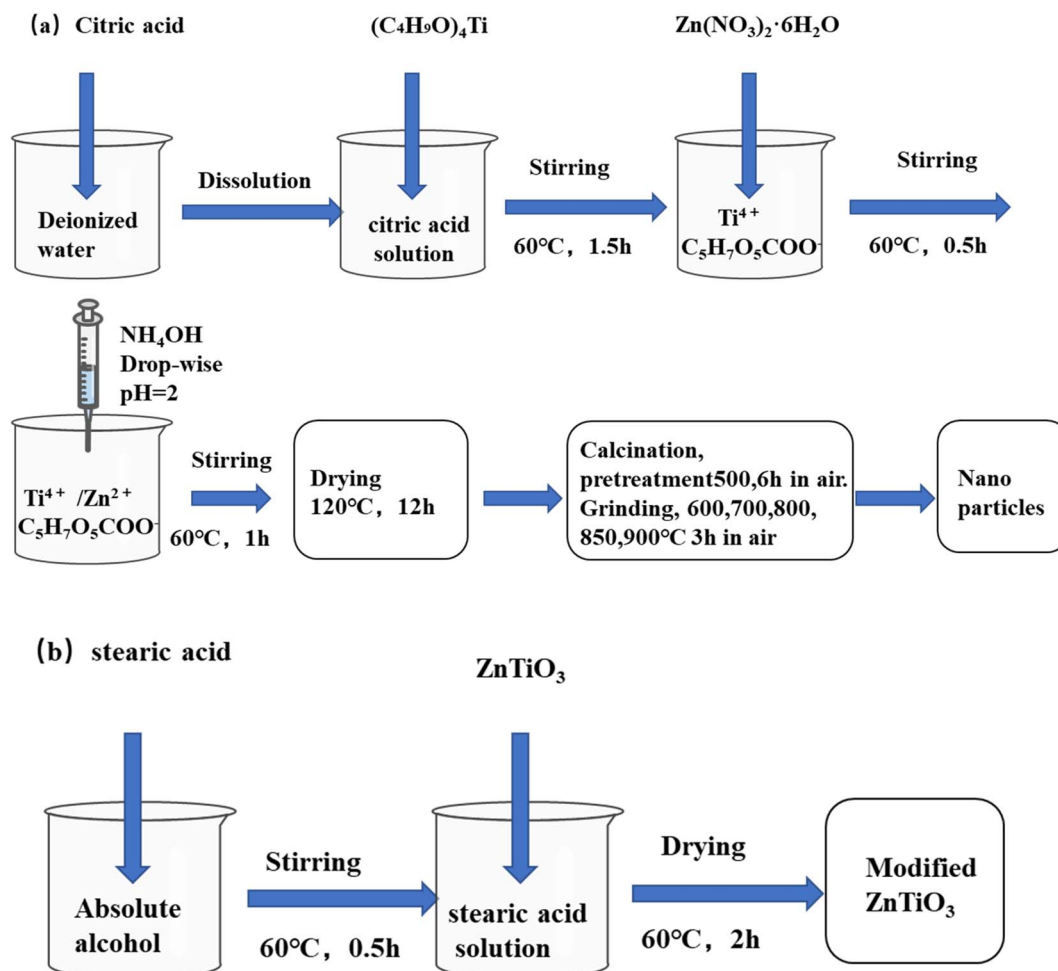


Fig. 1 Synthesis of nano ZT (a) sol-gel synthesis, (b) hydrophobically modified by stearic acid.

each group. After being placed at  $25^\circ C$  for 24 h, the performance of anti-graffiti was tested according to the Chinese standard of JG/T 304-2011.

### 3 Results and discussion

#### 3.1 Structure of ZT

Fig. 2 shows the XRD patterns of ZT calcined at 600, 700, 800, 850, and  $900^\circ C$ , respectively. When the temperature is raised to  $600^\circ C$ , it should be noted that there are no other compounds or free species except ZT in cubic form. This result indicates that cubic ZT has completed crystallization consistent with the standard card (JCPDS 39-0109). With the increased temperature, because the cubic phase ZT is unstable at high temperature and turns into hexagonal phase, the crystalline phase of hexagonal ZT was observed and the content gradually increased. When the temperature is at  $800^\circ C$ , except for a small amount of cubic ZT, which is the 220 ( $30.032^\circ$ ) diffraction peak of cubic phase. The hexagonal crystal system of ZT is close to pure phase accorded with the standard card (JCPDS 26-1500). When the calcination temperature rises from  $800^\circ C$  to  $900^\circ C$ , although the hexagonal ZT still dominates, the hexagonal ZT

decomposes into cubic crystal ( $Zn_2TiO_4$ ) and rutile ( $TiO_2$ ) at a much higher temperature. The peaks of rutile  $TiO_2$  and cubic  $Zn_2TiO_4$  were observed after the temperature up to  $900^\circ C$ . Therefore, there are peaks corresponding to cubic  $Zn_2TiO_4$  (JCPDS card no. 25-1164) and rutile  $TiO_2$  (JCPDS card no. 21-1276).

XPS and SEM were used to determine the surface composition and chemical state of ZT (Fig. S2†) and observe the morphological characteristics of synthetic pigments (Fig. S3†), respectively.

#### 3.2 SEM of SI and ZT/SI film

SEM was used to analyze the dispersion of inorganic particles in the polymer matrix. The fracture morphology of SI and ZT/SI composite films is shown in Fig. 3. Smooth surfaces and brittle fractures can be identified in pristine SI film. After adding M-ZT powder, white spots appeared on the surface and gradually increased with the increase of M-ZT content. When the mass fraction of U-ZT was 30 wt%, it was obvious that the U-ZT particles aggregated into massive particles and formed severe agglomeration. In contrast, 30 wt% M-ZT showed better



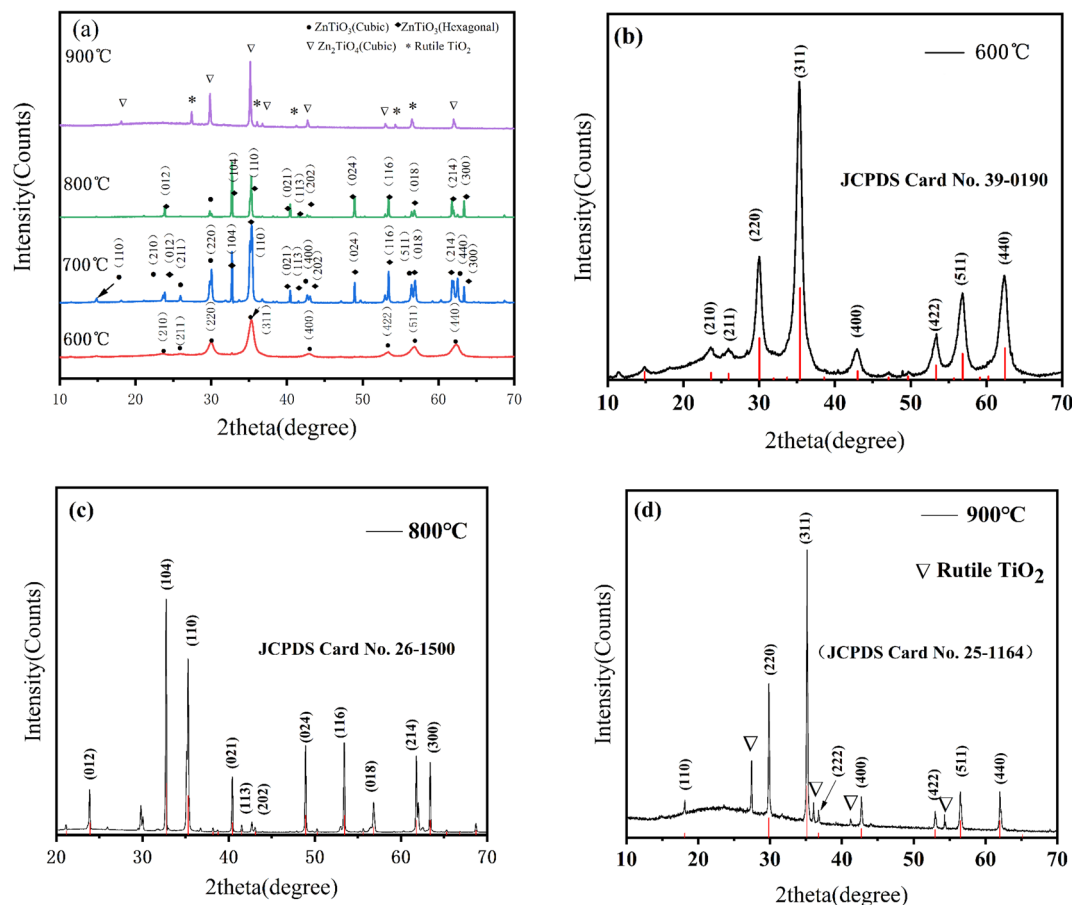


Fig. 2 XRD patterns of ZT calcined at different temperatures.

dispersion in silicone resin. This phenomenon indicates that stearic acid improves the compatibility of inorganic particles in the polymer matrix and promotes their interfacial adhesion.

### 3.3 Static contact angles and surface tension analysis

Generally speaking, the water contact angle can measure the hydrophilicity or hydrophobicity of a surface. If the contact

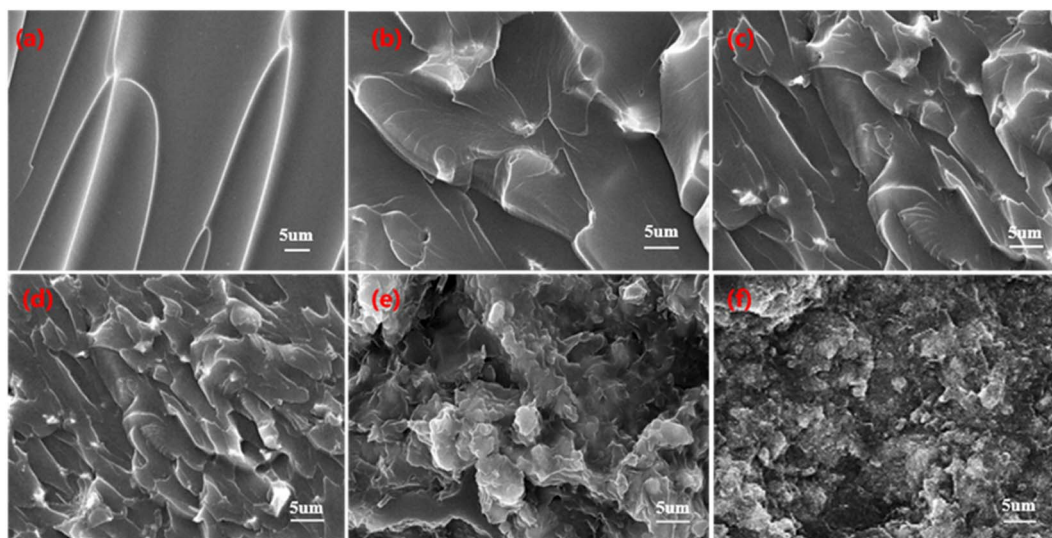


Fig. 3 SEM micrographs of fractured surfaces for SI and ZT/SI composite films. (a) SI, (b) 5 wt% M-ZT, (c) 10 wt% M-ZT, (d) 15 wt% M-ZT, (e) 30 wt% M-ZT, (f) 30 wt% ZT.





angle is more than 90°, it can be defined as hydrophobic, otherwise, it is hydrophilic. Hydrophobic coatings are usually considered one of the important indexes of self-cleaning coatings.<sup>27,28</sup> According to Owens and Wendt's method<sup>29,30</sup> as well as the Young equation, the surface energy of a solid is calculated. The formulas are as follows:

$$(1 + \cos \theta)\gamma_L = 2(\gamma_S^d\gamma_L^d)^{1/2} + 2(\gamma_S^p\gamma_L^p)^{1/2} \quad (1)$$

$$\gamma_S = \gamma_S^d + \gamma_S^p, \quad (2)$$

$\gamma_S^d$  and  $\gamma_S^p$  are liquid nonpolar and polar forces, respectively.  $\gamma_L^d$  and  $\gamma_L^p$  are solid nonpolar and polar forces, respectively.  $\gamma_S$  is the total surface tension.

The contact angles and surface tension of modified and unmodified ZT are given in Table 1. Unmodified ZnTiO<sub>3</sub> (U-ZT) has a very small water contact angle of 25, which signifies the hydrophilic surface of particles. For comparison, stearic acid modified with ZT performs a high contact angle of 155. It reflects the extremely strong hydrophobicity caused by the enrichment of organic groups on the surface of M-ZT.

The calculation results of surface tension of modified and unmodified ZT, including dispersive components and polar components are shown in Table 1. Compared to U-ZT, it was found that the surface tension of M-ZT was significantly reduced from 70.4 mJ m<sup>-2</sup> to 25.5 mJ m<sup>-2</sup>. The reason was that the stearic acid alkyl chain had been successfully adsorbed on the surface of ZT. The interaction between the surface and polar solvent is reduced and the hydrophobicity of the film is improved.

The static contact angles of the SI/ZT composite films are shown in Fig. 4. Compared with SI, the water contact angle of SI/M-ZT composite films gradually added with the increase of M-ZT loading. This is attributed to the M-ZT particles coated with stearic acid alkyl chains which made the films form a hydrophobic surface. In particular, 30 wt% M-ZT/SI film has the highest contact angle of 122° (20° higher than pure SI). On the contrary, the introduction of 30 wt% U-ZT reduces the water contact angle of the composite film to 95°, (7° lower than pure SI). The hydrophobic modification of the ZT contributes to the self-cleaning property of the film. This also indirectly confirms that the surface of ZT particles has been successfully converted from hydrophilic to hydrophobic.

### 3.4 Reflectance spectra of the ZT and ZT/SI film

The solar reflectances of the U-ZT and M-ZT particles were measured with a UV-VIS-NIR spectrophotometer from 300 to

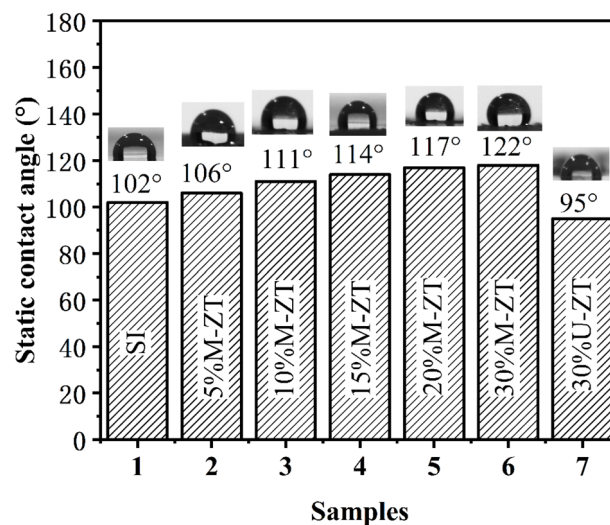


Fig. 4 The water contact angle of SI and ZT/SI composite films.

2500 nm. BaSO<sub>4</sub> was used as a reference. The NIR solar reflectance values ( $R^*$ ) were estimated according to the ASTM standard G173-03. The function  $R^*$  is given as follows:

$$R^* = \frac{\int_{\lambda_0}^{\lambda_1} r(\lambda) i(\lambda) d(\lambda)}{\lambda_1 - \lambda_0} \quad (3)$$

The fraction  $R^*$  of solar radiation incident at wavelengths between  $\lambda_0$  and  $\lambda_1$  reflected by a surface is the irradiance-weighted average of its spectral reflectance  $r(\lambda)$ .

$$S = 0.05R_{UV} + 0.43R_{VIS} + 0.52R_{NIR} \quad (4)$$

where  $i(\lambda)$  is the solar spectral irradiance. Irradiance-weighted average reflectances include solar reflectance  $S$  (0.3–2.5 mm), UV reflectance  $U$  (0.3–0.4 mm), visible reflectance  $V$  (0.4–0.8 mm), and NIR reflectance  $N$  (0.8–2.5 mm). The solar reflectance of a surface may be computed as the weighted average of its UV, visible, and NIR reflectances. The distribution mentioned above of solar power (5% UV, 43% visible, and 52% NIR) yields.

The solar reflectance spectrum and corresponding reflectance spectrum calculation of M-ZT and U-ZT are shown in Fig. 5. It can be seen from the figure that M-ZT and U-ZT show high reflectivity in the visible and near-infrared regions. Although the spectrum shows that the reflectivity of M-ZT is slightly lower than that of U-ZT, decreases by 0.7% in the visible light band, 2.1% in the near-infrared outer band, and 1.4% in the total solar spectral band. The magnitude of the reduction is small, and considering the improvement in self-cleaning performance brought about by the improved contact angle, the application range of the coating is increased.

Solar reflectance is very important for evaluating the cooling performance of materials. The solar reflectance of SI and its composite films and the solar reflectance calculation in each wavelength band is shown in Fig. 6. The solar reflectance of the 30% M-ZT/SI coating is much higher than that of SI, and the reflectances in the ultraviolet, visible, and near-infrared bands

Table 1 Contact angles and surface tension of modified and unmodified ZT

	Contact angle		Surface tension (mJ m <sup>-2</sup> )		
	Deionized water	Diiodomethane	$\gamma_S^d$	$\gamma_S^p$	$\gamma_S$
U-ZT	25	31	35.4	35.0	70.4
M-ZT	155	81	20.6	4.9	25.5



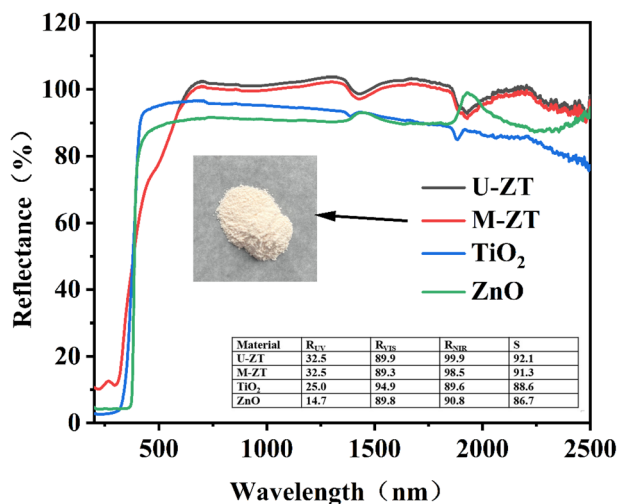


Fig. 5 Solar reflectance spectra of U-ZT, M-ZT, TiO<sub>2</sub>, and ZnO.

are 27.4, 82.8, and 81.2, respectively. Due to the strong UV absorption ability of ZT particles. Because of this reason, coatings can be effectively protected. As we all know, the energy of ultraviolet photons is similar to the chemical bond energy of some polymers. Therefore, the aging degradation of organic materials and the loss of mechanical strength are related to ultraviolet radiation in the atmosphere.<sup>31</sup> To sum up, the 30% M-ZT/SI coating has the best sunlight reflection performance.

### 3.5 Evaluate the actual cooling effect of ZT/SI film

In order to study the thermal insulation properties of the film, the ZT/SI coating is applied to the aluminum plate. Set up special instruments for testing thermal insulation performance. The schematic diagram of the experimental device is shown in Fig. 7. The device consisted of a thermal box, a digital thermometer, and an infrared lamp. The thermal box was made of polystyrene foam board (except the top opening) and equipped

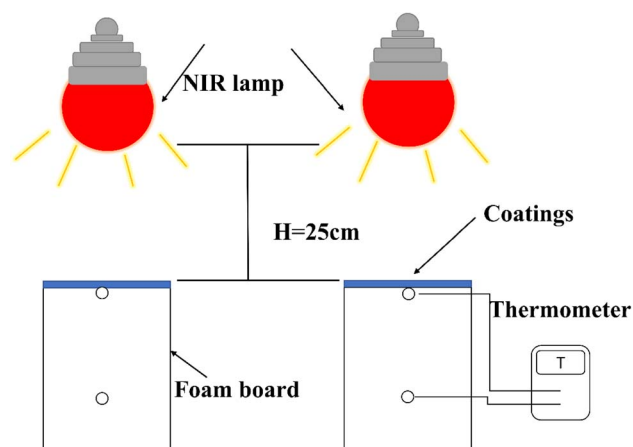


Fig. 7 Insulation test device.

with a 300 W infrared lamp. The aluminum plate was placed on top of the box in contact with the thermometer. The air temperature was maintained at 25 °C by air conditioning. The temperature of the inner surface of the aluminum plate and inside the thermal box is recorded in real-time.

The inner surface temperature of the film and the air temperature of the foam box was recorded in Fig. 8. It can be seen from Fig. 8a that the inner surface temperature of the 30% M-ZT/SI coating shows an upward trend, reaching 63.3 °C. The SI coating temperature rises to 70.1 °C, and the temperature difference reaches 6.8 °C. The 30% M-ZT/SI has strong near-infrared light reflection ability, which reduces energy absorption, and the thermal insulation performance is better than SI.

Fig. 8b shows the internal air temperature of the foam box coated with two coatings. It can be seen that, after 60 minutes, the temperatures of M-ZT/SI and SI were stabilized at 38.5 °C and 42.4 °C, and the temperature difference could reach 3.9 °C. This indicates that M-ZT can significantly enhance the cooling effect of SI coatings, and have the potential to be applied to residential roofing materials to save energy and improve thermal comfort.

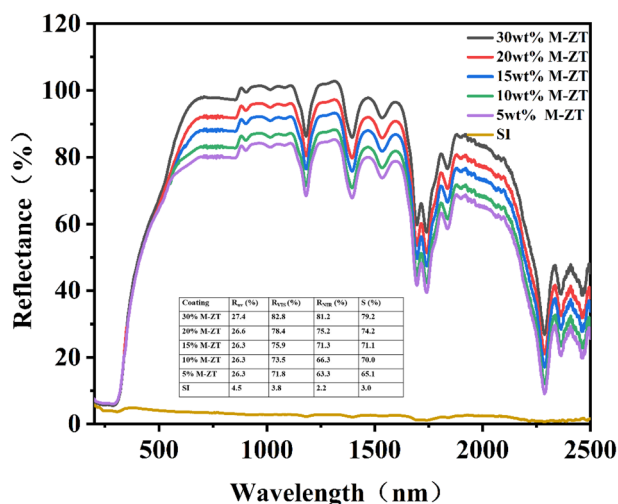


Fig. 6 Solar reflectance spectra of SI and ZT/SI composite film.

### 3.6 High-low temperature cycles test and UV radiation resistance

Because solar reflective coatings are exposed to harsh outdoor conditions for long periods, they must be highly resistant to high-low temperatures and ultraviolet radiation. Therefore, high-low temperature cycles and UV aging tests were carried out on the reflective thermal insulation coatings. The data is recorded in Fig. 9. It can be seen that the contact angle of the film changes little and still maintains its hydrophobicity when the coating is cooled and heated 10 times in 4 hours between −25 °C and 60 °C. At the same time, the coating still has hydrophobicity and the change of gloss is not obvious after 100 h of UV irradiation experiment. Gloss changes are closely related to the degradation degree of the coating during accelerated aging. So the coating has excellent anti-ultraviolet aging performance. Chemical shielding ability of coatings (Fig. S4†).



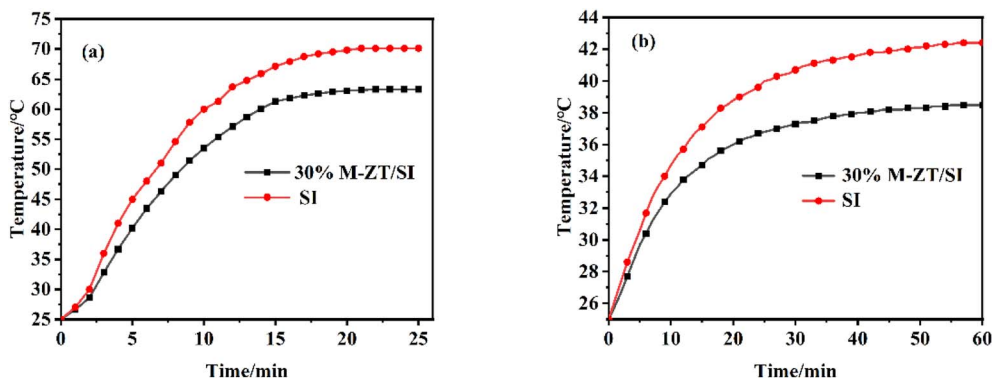


Fig. 8 The temperature (a) the inner surface of films, (b) the interior air of the foam boxes.

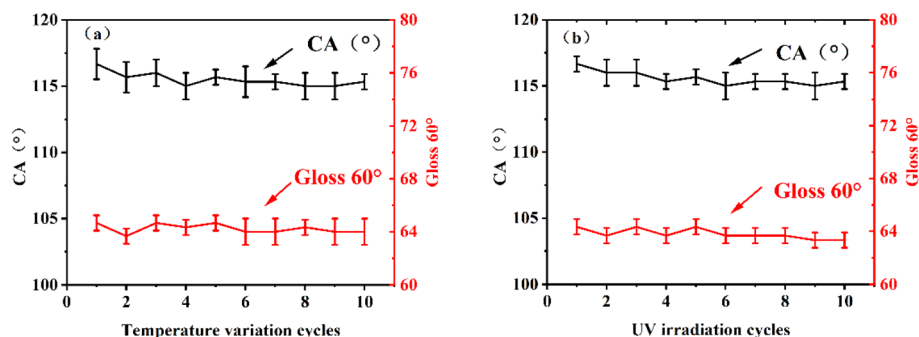


Fig. 9 Weathering test of coatings, (a) high-low temperature cycles test, (b) UV radiation resistance.

### 3.7 Energy consumption analysis

Shanghai has a subtropical monsoon climate, with hot summers all year round, and air conditioners consume a lot of energy. Therefore, the energy consumption in Shanghai from June to August was simulated by the EnergyPlus software. The influence of the high near-infrared reflective coating on the outer wall and roof on energy consumption was analyzed.

First, a double-layered model building of about 200 m<sup>2</sup> was built using OpenStudio software. The roof adopts a pitched roof, and windows and doors are also installed. The building adopts an HVAC system (Ideal Loads Air System) for cooling and heating. The heating temperature and the cooling temperature of the building were set to 18 °C and 26 °C. When the indoor temperature is lower than 18 °C or higher than 26 °C, the HVAC system auto starts. The indoor personnel density is 0.111 persons per m<sup>2</sup>. A load of electrical equipment and lighting equipment is 10 W m<sup>-2</sup>. The coating thickness is 150 μm. The other parameters are default values. The energy consumption of the air-conditioning system is simulated and analyzed. The building model is shown in Fig. 10.

The results of energy consumption analysis are shown in Table 2, compared with the cement exterior wall of the building, the energy consumption of a building coated with M-ZT reflective coating is reduced by 1.8 kW h m<sup>-2</sup>. And it can save 10.29 dollars in electricity bills every month.

### 3.8 Anti-graffiti analysis of ZT/SI film

Due to the low surface energy and excellent liquid repellency of M-ZT/SI coatings, it is indicated that they can be used for anti-graffiti.

According to the order of cleaning ability from weak to strong, a cotton cloth, a wireless cotton cloth soaked with 1% water-based weak cleaning agent, a lint-free cotton cloth soaked with the orange bridge cleaning agent, and a lint-free cotton cloth full of alcohol in a set of tests were used. The graffiti marks



Fig. 10 Building model established by OpenStudio.

Table 2 Solar reflectance and simulated results of bare cement and the two coatings

Coating	Visible reflectance (%)	Near-infrared (%)	Solar reflectance (%)	Electricity (kW h m <sup>-2</sup> )
Cement	30.0	37.0	35.0	18.01
M-ZT/SI	82.8	81.2	79.2	16.21

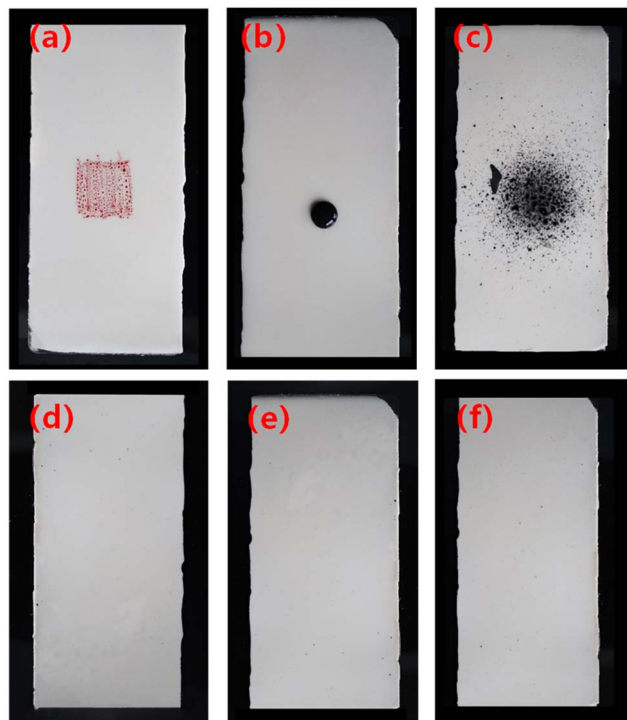


Fig. 11 Anti-graffiti tests. (a) Oily red marker, (b) water-based black ink, (c) solvent-based black acrylic spray paint; (d–f) respectively for the coating after wiping.

Table 3 The grades of anti-graffiti

Grade	Graffiti removal
Level 1	Removable with dry lint-free cotton cloth
Level 2	Removable with 1% neutral water-based weak cleaning agent
Level 3	Removable with a citrus-based cleaner
Level 4	Removable with absolute ethanol
Not clearable	None of the four cleaning materials can be removed

on the aluminum plate were wiped back and forth 25 times with a wiping pressure of about 1.5 kg. If two of the three test panels do not leave obvious graffiti marks, and the coating shows no noticeable loss of gloss and discoloration, the cleaning process is over. Otherwise, replace a set of test panels and clean them with a stronger grade of cleaning material (Table 3).

The results obtained by wiping three different graffiti with 1% neutral water-based weak cleaning agent show that all three

kinds of graffiti can be erased, and the coating has no obvious loss of gloss and discoloration. According to the evaluation of the cleaning level, it can reach the second level. From Fig. 11, it can be seen that the red smear of the marker pen and the black smear of the ink shrink rather than spread to the surface of the coating, indicating that the coating exhibits significant repulsion to water-based and oil-based stains. Graffiti material acrylic spray paint has the characteristics of strong adhesion and rapid drying. It is difficult to clean up on ordinary coatings, but it can be completely erased on the coating to be tested, indicating that the coating is suitable for use to prevent graffiti. Specific graffiti wiping video visible Movies S1–S3.†

## 4 Conclusion

In this study, ZT particles were used to improve the cooling performance of SI. The effects of the content of ZT and M-ZT particles and surface hydrophobic modification on the SI dispersion properties were investigated. The following conclusions can be drawn: the dispersibility of M-ZT in the coating is better than that of ZT. Therefore, surface modification of ZT with stearic acid to obtain a hydrophobic surface can effectively improve the dispersibility of inorganic particles in SI matrix. Meanwhile, different additions of M-ZT can increase the reflectance of the coating from 3.0% to 79.2%, and a significant reduction of 6.8 °C can be achieved. The coating remains glossy and hydrophobic after high and low-temperature cycling and UV aging tests. EnergyPlus software simulated the energy consumption of an air conditioning system, and the simulations showed that homeowners could save \$10.29 a month by applying an energy-efficient paint consisting of ZT to the walls and roof of their homes. In addition, the coating exhibits remarkable anti-graffiti performance.

## Author contributions

Conceptualization, S. W. and J. W.; methodology, S. W.; visualization, S. W.; validation, H. L.; formal analysis, C. X. and L. S.; data curation, H. L., C. X. and S. L.; writing-original draft preparation, S. W.; writing-review and editing, S. W., J. W. and S. W. (Shaoguo Wen); supervision, J. W.; project administration, D. M. All authors have read and agreed to the published version of the manuscript.

## Conflicts of interest

The authors declare that they have no known competing financial interests or personal relationships that could have appeared to influence the work reported in this paper.





## Acknowledgements

This research did not receive any specific grant from funding agencies in the public, commercial, or not-for-profit sectors.

## References

- 1 S. Mirrahimi, M. F. Mohamed, L. C. Haw and et al, ., The effect of building envelope on the thermal comfort and energy saving for high-rise buildings in hot-humid climate, *Renewable Sustainable Energy Rev.*, 2016, **53**, 1508–1519.
- 2 E. Enríquez, V. Fuertes, M. J. Cabrera and et al, ., New strategy to mitigate urban heat island effect: energy saving by combining high albedo and low thermal diffusivity in glass ceramic materials, *Sol. Energy*, 2017, **149**, 114–124.
- 3 D. L. Andrews, *Encyclopedia of applied spectroscopy*, Wiley-VCH, Weinheim, Germany, 2009.
- 4 I. Yüksel, Global warming and renewable energy sources for sustainable development in Turkey, *Renewable Energy*, 2008, **33**(4), 802–812.
- 5 M. Baneshi and S. Maruyama, The impacts of applying typical and aesthetically-thermally optimized TiO<sub>2</sub> pigmented coatings on cooling and heating load demands of a typical residential building in various climates of Iran, *Energy Build.*, 2016, **113**, 99–111.
- 6 C. Ding, A. Han, M. Ye and et al, ., Synthesis and characterization of a series of new green solar heat-reflective pigments: Cr-doped BiPO<sub>4</sub> and its effect on the aging resistance of PMMA (poly(methyl methacrylate)), *Sol. Energy Mater. Sol. Cells*, 2019, **191**, 427–436.
- 7 J. Long, C. Jiang, J. Zhu and et al, ., Controlled TiO<sub>2</sub> coating on hollow glass microspheres and their reflective thermal insulation properties, *Particuology*, 2020, **49**, 33–39.
- 8 Y. Bao, Q. L. Kang and J. Z. Ma, Structural regulation of hollow spherical TiO<sub>2</sub> by varying titanium source amount and their thermal insulation property, *Colloids Surf., A*, 2018, **537**, 69–75.
- 9 G. Wei, J. Ding, T. Zhang and et al, ., *In situ* fabrication of ZnO nanorods/Ag hybrid film with high mid-infrared reflectance for applications in energy efficient windows, *Opt. Mater.*, 2019, **94**, 322–329.
- 10 I. S. Bayer, Superhydrophobic Coatings from Ecofriendly Materials and Processes: A Review, *Adv. Mater. Interfaces*, 2020, **7**(13), 2000095.
- 11 S. Lei, H. Fan, X. Ren and et al, ., Microstructure, phase evolution and interfacial effects in a new Zn<sub>0.9</sub>Mg<sub>0.1</sub>TiO<sub>3</sub>-ZnNb<sub>2</sub>O<sub>6</sub> ceramic system with greatly induced improvement in microwave dielectric properties, *Scr. Mater.*, 2018, **146**, 154–159.
- 12 D. P. Dutta, A. Singh and A. K. Tyagi, Ag doped and Ag dispersed nano ZnTiO<sub>3</sub>: improved photocatalytic organic pollutant degradation under solar irradiation and antibacterial activity, *J. Environ. Chem. Eng.*, 2014, **2**(4), 2177–2187.
- 13 R. Abirami, C. R. Kalaiselvi, L. Kungumadevi and et al, ., Synthesis and characterization of ZnTiO<sub>3</sub> and Ag doped ZnTiO<sub>3</sub> perovskite nanoparticles and their enhanced photocatalytic and antibacterial activity, *J. Solid State Chem.*, 2020, **281**, 121019.
- 14 J. Yu, D. Li, L. Zhu and et al, ., Application of ZnTiO<sub>3</sub> in quantum-dot-sensitized solar cells and numerical simulations using first-principles theory, *J. Alloys Compd.*, 2016, **681**, 88–95.
- 15 W. M. Reese, P. Burch, A. B. Korpusik and et al, ., Facile Macrocyclic Polyphenol Barrier Coatings for PDMS Microfluidic Devices, *Adv. Funct. Mater.*, 2020, **30**(48), 2001274.
- 16 A. Vitale, S. Touzeau, F. Sun and et al, ., Compositional Gradients in Siloxane Copolymers by Photocontrolled Surface Segregation, *Macromolecules*, 2018, **51**(11), 4023–4031.
- 17 H. Cheng, F. Wang, J. Ou and et al, ., Solar reflective coatings with luminescence and self-cleaning function, *Surf. Interfaces*, 2021, **26**, 101325.
- 18 G.-Z. Li, G.-G. Wang, Y.-W. Cai and et al, ., A high-performance transparent and flexible triboelectric nanogenerator based on hydrophobic composite films, *Nano Energy*, 2020, **75**, 104918.
- 19 D. Wang, X. Zhou, R. Song and et al, ., Freestanding silver/polypyrrole composite film for multifunctional sensor with biomimetic micropattern for physiological signals monitoring, *Chem. Eng. J.*, 2021, **404**, 126940.
- 20 Z. Song, J. Qin, J. Qu and et al, ., A systematic investigation of the factors affecting the optical properties of near infrared transmitting cool non-white coatings, *Sol. Energy Mater. Sol. Cells*, 2014, **125**, 206–214.
- 21 Y.-D. Xu, Z.-Y. Zhu, T.-Z. Xu and et al, ., Fabrication and characterization of robust hydrophobic lotus leaf-like surface on Si<sub>3</sub>N<sub>4</sub> porous membrane *via* polymer-derived SiNCO inorganic nanoparticle modification, *Ceram. Int.*, 2018, **44**(14), 16443–16449.
- 22 Y. Zhu, G. C. Allen, J. M. Adams and et al, ., Statistical analysis of particle dispersion in a PE/TiO<sub>2</sub> nanocomposite film, *Compos. Struct.*, 2010, **92**(9), 2203–2207.
- 23 Y. Si, Z. Guo and W. Liu, A Robust Epoxy Resins @ Stearic Acid-Mg(OH)<sub>2</sub> Micronanosheet Superhydrophobic Omnipotent Protective Coating for Real-Life Applications, *ACS Appl. Mater. Interfaces*, 2016, **8**(25), 16511–16520.
- 24 L. Xu, Z. Geng, J. He and et al, ., Mechanically Robust, Thermally Stable, Broadband Antireflective, and Superhydrophobic Thin Films on Glass Substrates, *ACS Appl. Mater. Interfaces*, 2014, **6**(12), 9029–9035.
- 25 F. Yan, X. Zhang, F. Liu and et al, ., Adjusting the properties of silicone rubber filled with nanosilica by changing the surface organic groups of nanosilica, *Composites, Part B*, 2015, **75**, 47–52.
- 26 J. Lv, M. Tang, R. Quan and et al, ., Synthesis of solar heat-reflective ZnTiO<sub>3</sub> pigments with novel roof cooling effect, *Ceram. Int.*, 2019, **45**(12), 15768–15771.
- 27 V. A. Ganesh, H. K. Raut, A. S. Nair and et al, ., A review on self-cleaning coatings, *J. Mater. Chem.*, 2011, **21**(41), 16304–16322.



- 28 J. Jeevahan, M. Chandrasekaran, G. Britto Joseph and et al, ., Superhydrophobic surfaces: a review on fundamentals, applications, and challenges, *J. Coat. Technol. Res.*, 2018, **15**(2), 231–250.
- 29 D. K. Owens and R. C. Wendt, Estimation of the surface free energy of polymers, *J. Appl. Polym. Sci.*, 1969, **13**(8), 1741–1747.
- 30 F. Piscitelli, F. Tescione, L. Mazzola and et al, ., On a simplified method to produce hydrophobic coatings for aeronautical applications, *Appl. Surf. Sci.*, 2019, **472**, 71–81.
- 31 N. S. Bora, B. Mazumder and P. Chattopadhyay, Prospects of topical protection from ultraviolet radiation exposure: a critical review on the juxtaposition of the benefits and risks involved with the use of chemoprotective agents, *J. Dermatol. Treat.*, 2018, **29**(3), 256–268.

